Estimating Drag and Heating Coefficients for Hollow Reentry Objects in Transitional Flow Using DSMC

Jeremiah J. Marichalar[(1)] and Chris L. Ostrom[(2)]

[(1)] GeoControl Systems - Jacobs JETS Contract, NASA Johnson Space Center, Mail Code EG3-16, 2101 NASA Pkwy., Houston, TX 77058, USA, jeremiah.j.marichalar@nasa.gov
[(2)] HX5 – Jacobs JETS Contract, NASA Johnson Space Center, Mail Code XI5-9E, 2101 NASA Pkwy., Houston, TX 77058, USA, christopher.l.ostrom@nasa.gov

ABSTRACT

In NASA's Object Reentry Survival Analysis Tool (ORSAT), aerodynamic drag and aerothermal heating coefficients are computed for each of the free-molecular, continuum, and transitional flow regimes using analytical and semi-analytical methods. These methods are typically limited to convex, blunt objects (such as spheres) and are applied to other objects such as boxes and cylinders using multiplicative "shape factors" to account for the different behavior.

Previous literature has analyzed the aerodynamic and aerothermodynamic properties of flow around sharp-edged objects like boxes and cylinders in transitional flow, though only those objects with solid external boundaries. However, many reentry objects we have encountered in real spacecraft have been hollow (*i.e.*, with the potential to allow flow through them). We present here preliminary results from analyses performed using the NASA Direct Simulation Monte Carlo (DSMC) Analysis Code (DAC) on hollow cylinders and boxes (with varying wall thickness-diameter ratio).

1 INTRODUCTION

Aerodynamic and aerothermodynamic coefficients used in reentry survivability analysis software codes, such as the Object Reentry Survival Analysis Tool (ORSAT) developed for use by the NASA Orbital Debris Program Office, have historically been determined through experimental data (mainly for subsonic, transonic, and low supersonic regimes) and analytical approximations (high hypersonic or free molecular flow). The behavior of objects in rarefied and transitional flows (where the flow is dilute enough that continuum mechanics breaks down and statistical methods must be used) has been analyzed using blending functions, which may consist of combinations of trigonometric functions, logarithms and exponentials, and polynomials. These blending functions interpolate coefficient values from the free molecular and continuum regimes as a function solely of the Knudsen number (Kn), a measure of how dilute a gas flow is around an object (see Eq. 1, where λ is the mean free path, or how far a gas particle travels on average between collisions, and L is the characteristic length of the object).

$$Kn = \frac{\lambda}{L} \qquad \text{(Eq. 1)}$$

Continuum flow is assumed to occur for flows where Kn is less than 0.001; free molecular flow is typically assumed to occur where Kn is greater than 10; the region between these limits is called the transitional, or rarefied, flow regime. A graphical depiction of the different methods used to compute flows with varying Kn is seen in Fig. 1. It is interesting to note that the statistical models are valid for all flow regimes, from free molecular to continuum, though it is extremely computationally expensive to use these methods for denser gas flows.

ORSAT analysis requires the assignment of components to several shape primitives, namely: boxes, flat plates, spheres, cylinders, disks, rings, sharp and blunt cones, and frusta. The box and cylinder models are the focus of the present work. The box model in ORSAT assumes a constant drag coefficient of 1.42 in continuum flow (*i.e.*, Kn < 0.001) and a constant free-molecular flow (Kn > 10) drag coefficient of 2.55 [1]. These values are interpolated using Eq. 2 for the transitional flow regime (Kn between 0.001 and 10) [2]. A similar process is used for computing drag coefficients for cylinders, replacing the continuum and free molecular drag coefficients with 1.22 and 2.0, respectively [1]. Other models for drag and heating coefficients in transition flow can be found in References [3] through [6].

$$C_{D,trans} = C_{D,C} + \left(C_{D,FM} - C_{D,C}\right) * \left[\sin\left(\pi\left(\frac{1}{2} + \frac{1}{4}\log Kn\right)\right)\right]^3 \qquad \text{(Eq. 2)}$$

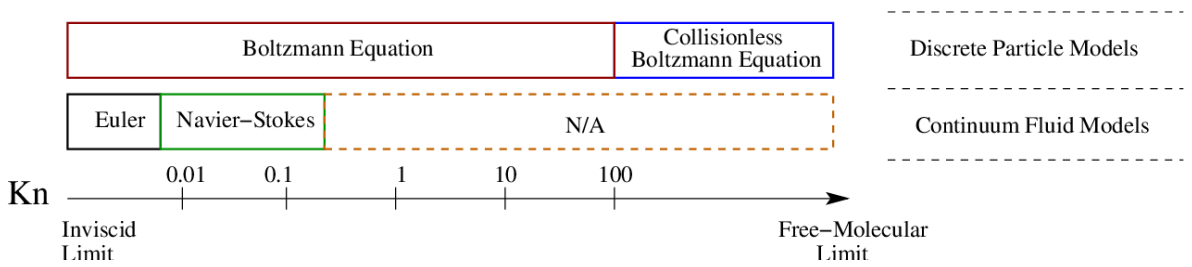

Fig. 1. Solution methods for gas flows with varying Kn.

Research has been done by other groups to develop new estimates of these drag and heating coefficients for the continuum hypersonic through transitional regimes using computational fluid dynamics (CFD) and direct simulation Monte Carlo (DSMC) tools. We will discuss first the work by Mehta, *et al*. [7], in which spheres, cubes, and right circular cylinders were run through CFD and DSMC simulations to establish an improved basis upon which to interpolate drag and heating coefficients in the transitional flow regime. These simulations were all conducted assuming a constant ram-facing attitude. Of particular interest from that work is the heat flux distribution on the ram faces of the cube and cylinder, which have no purely analytical form. The crucial modeling step that can be taken away from this work is that the heat flux distribution can be described as a multiplier on top of the stagnation-point heat flux, which is in turn solely a function of Kn.

Figures 2 and 3 show comparisons of heat flux computed using DSMC and the result of the heat flux distribution model (used in the Free Open Source Tool for Reentry of Asteroids and Debris [FOSTRAD]) derived from the DSMC data (reproduced from [7]). The heat flux coefficient C_h used in the figures (and in the following sections of this work) is defined by Eq. 3, where Q is the local heat flux at a position on the body, ρ is the freestream density, and v is the freestream speed.

$$C_h = \frac{2Q}{\rho v^3} \qquad \text{(Eq. 3)}$$

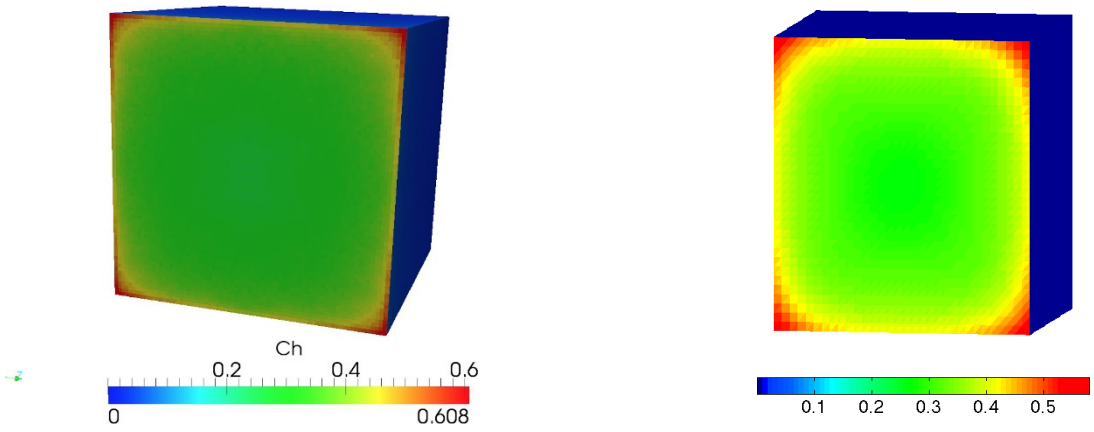

Fig. 2. Comparison of cube surface heat flux distributions computed with DSMC (left) and FOSTRAD (right) at Kn = 0.08.

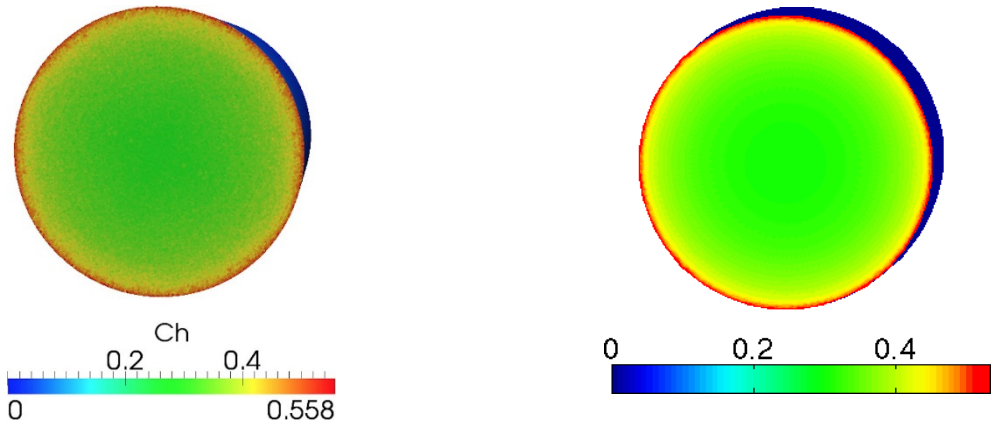

Fig. 3. Comparison of cylinder surface heat flux distributions computed with DSMC (left) and model (right) at Kn = 0.08.

Next, we will discuss the work done by Scanlon, *et al*. [8], in which CFD and DSMC are used to compute drag force and total heat flux on solid and hollow cylinders at several angles of attack. This work extended the usability of DSMC and CFD simulations to rarefied flows for hollow objects, which are typically modeled with the same physics as solid objects, with the only modification being a different reference area to which the drag force and heat flux are applied. Fig. 4 shows the surface heat flux distribution for a solid and hollow cylinder at 45° angle of attack (reproduced from [8]). It is immediately clear that there is indeed flow through the hollow cylinders (and heating on the inner wall of the cylinders).

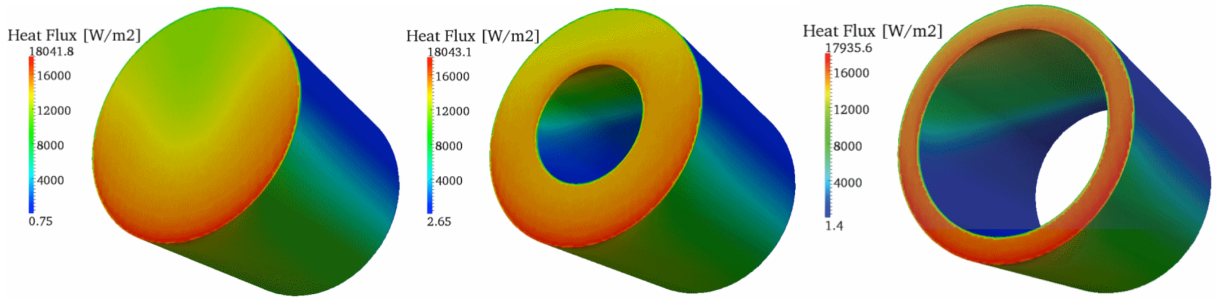

Fig. 4. Comparison of DSMC cylinder surface heat flux distributions, with varying wall thickness: 100% (left), 50% (middle), 20% (right)

References [7] and [8] form a foundation on which the present work continues: the use of DSMC simulations of transitional gas flows to produce simplified measures, including drag and heating coefficients, as well as a "hollowness" criterion, for use in existing reentry survivability analysis software.

2 APPROACH

Cylinders and boxes (square rectangular prisms) of varying length, wall thickness, and outer diameter (or width) were modeled with the NASA DSMC Analysis Code (DAC) [9]. The DSMC method [10] models the motions and collisions of representative molecules in the flow field and uses statistical sampling to compute the quantities of interest. The DAC software is a parallel implementation of the DSMC method that was developed at the NASA Johnson Space Center. DAC has been used extensively to simulate high altitude re-entry for a number of vehicles including the U.S. Space Shuttle and the Orion crew module, and has been validated against available flight data. The use of the virtual sub-cell DSMC collision method along with fundamental best-practices ensures that the DAC software achieves physically accurate results [3].

The case matrix for this hollow body study consisted of 81 cylinder cases and 81 box cases. Each shape was simulated in three scenarios: with angle of attack of 0, 45, or 90 degrees (defined as α, in Fig. 5). A single altitude and free stream condition were assumed; the simulation conditions are summarized in Table 1. For each shape, nine unique geometries were constructed based on length-to-diameter (L/D) ratios of 1.0, 0.5, and 0.1 and inner-

diameter-to-outer-diameter (ID/OD) ratios of 0.95, 0.5, and 0.1. Kn variation was achieved by scaling the geometry diameter (or width) for the nine unique geometries.

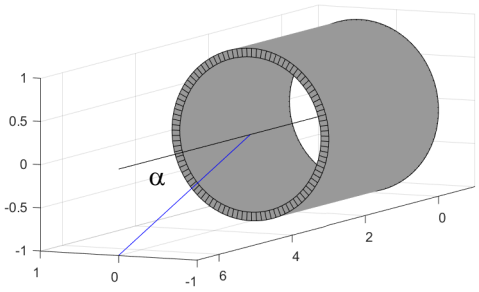

Fig. 5. Angle of attack definition.

Table 1. DSMC Simulation Conditions.

Quantity	Values
Altitude (km)	111.375
Freestream Speed (m/s)	7800
Freestream Density (kg/m3)	7.61E-08
Freestream Temperature (K)	256.5
Wall Temperature (K)	300
Knudsen Number	0.2, 1, 10
Outer Diameter (m)	0.1, 1, 5
ID/OD ratio	0.1, 0.5, 0.95
Angle of attack (°)	0, 45, 90
Fineness ratio (Length/Diameter)	0.1, 0.5, 1

A goal of the present work is to determine when a hollow object can be modeled as a solid object with a smaller area presented to the flow or as a hollow object with its own drag model. To this end, two hollowness criteria (HC) were developed (Eqs. 4 and 5). These are measures of the mass flow through the hollow object, (1) relative to the mass flow rate through a freestream streamtube of the same size as the hole in the object, and (2) relative to the mass flow rate through a freestream streamtube the same size as the entire object. As criterion 2 approaches unity, the object has a smaller and smaller blocking effect on the flow through the hole, and may be treated as an 'unrolled' object (*e.g.*, a ring may be unrolled into a long cylinder, or a short tube into a long flat plate.)

$$HC_1 = \frac{\dot{m}_{thru}}{\rho_\infty v_\infty A_{inner}} \qquad \text{(Eq. 4)}$$

$$HC_2 = \frac{\dot{m}_{thru}}{\rho_\infty v_\infty A_{outer}} \qquad \text{(Eq. 5)}$$

3 RESULTS

The full case matrix consists of 81 simulations for each hollow body shape. Surface heat flux distributions and flowfield-contour plots for all of the DSMC simulations were created using the DAC post-processing tools. A sample of the surface heat flux distribution plots for each shape is presented for brevity. Figures 6 and 7 display the surface heat flux distributions for the DSMC simulations of the cylindrical hollow bodies at 45° angle-of-attack.

Figure 6 compares surface heat flux for a constant length and varying wall thickness while Fig. 7 compares the surface heat flux distributions for varying object length and a constant wall thickness.

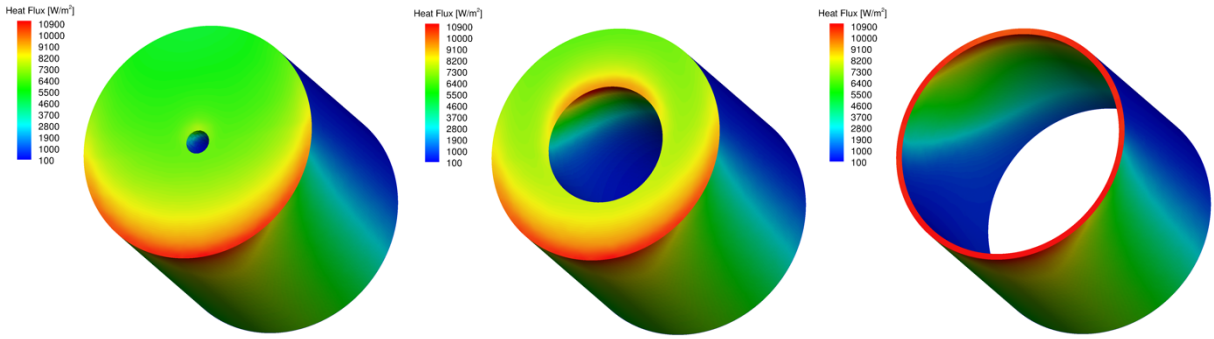

Fig. 6. Comparison of DSMC cylinder surface heat flux distributions with varying ID/OD ratio: 0.1 (left), 0.5 (middle), 0.95 (right)

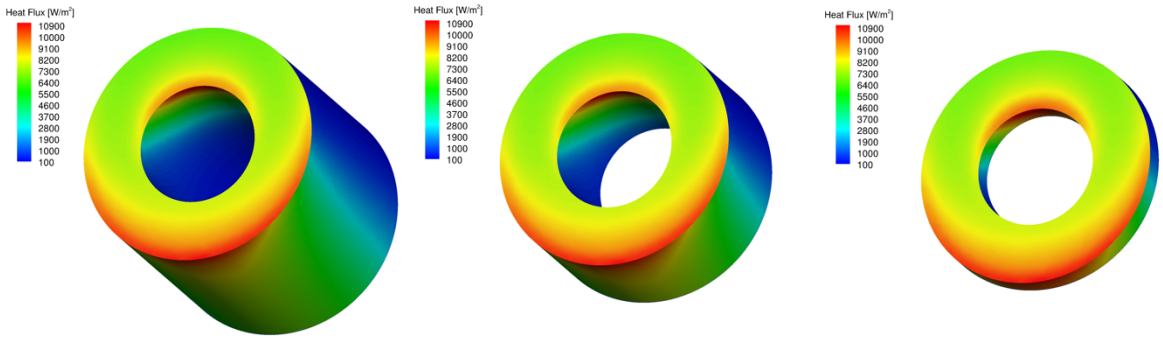

Fig. 7. Comparison of DSMC cylinder surface heat flux distributions with varying L/D ratio: 1.0 (left), 0.5 (middle), 0.1 (right)

Similarly, Figs. 8 and 9 display the surface heat flux distributions for the DSMC simulations of the square rectangular prism hollow bodies at 45° angle-of-attack. Figure 8 compares surface heat flux for a constant length and varying wall thickness while Fig. 9 compares the surface heat flux distributions for varying wall length and a constant wall thickness.

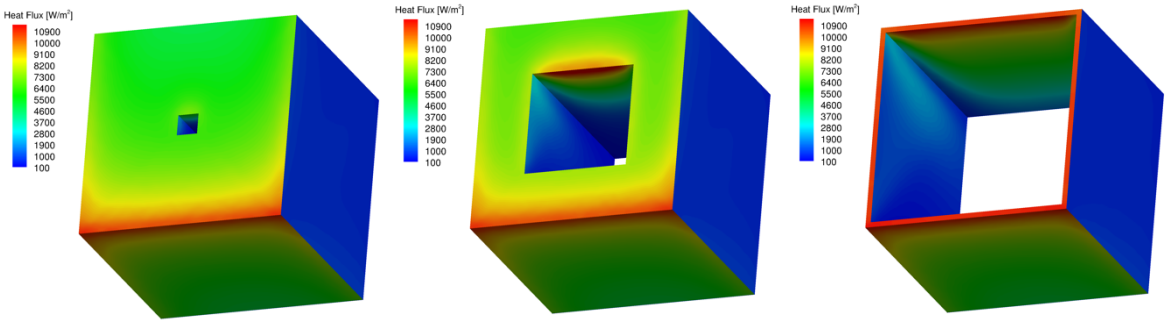

Fig. 8. Comparison of DSMC square rectangular prism surface heat flux distributions with varying ID/OD ratio: 0.1 (left), 0.5 (middle), 0.95 (right)

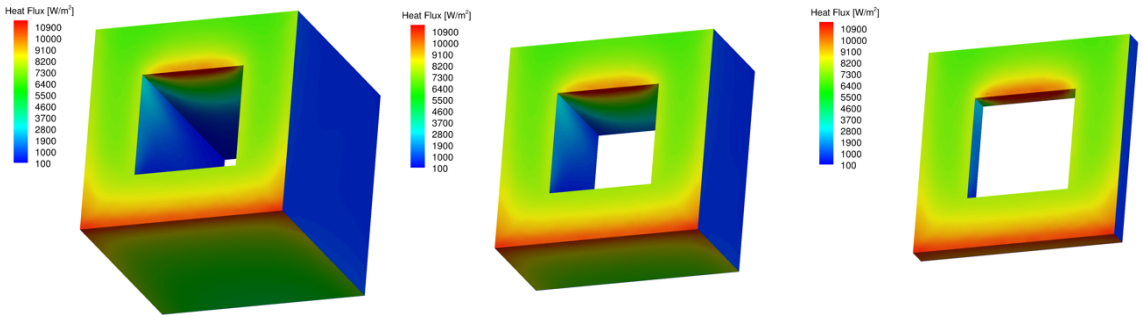

Fig. 9. Comparison of DSMC square rectangular prism surface heat flux distributions with varying L/D ratio: 1.0 (left), 0.5 (middle), 0.1 (right)

The heating and drag coefficients, along with the "hollowness" criteria, were extracted from the DSMC simulations and tabulated for each case in Appendix A. It is interesting to note that the values of HC_1 are usually greater than one (*i.e.*, the mass flow through the hollow object is greater than through a streamtube of the same size and shape) for the cases where $\alpha = 0°$ and $Kn < 10$. This effect was not anticipated; as the flow was expected to follow a similar path as over a solid object, at least until the hole became large with respect to the outer size. However, after examining the stagnation conditions at the ram and aft surfaces of the object, it becomes clearer that there can be significant flow through the hollow object, due to both compressibility and viscous effects, even in this rarefied flow. It is also important to note that even if the mass flow through the object is greater than through an equivalent freestream streamtube, the momentum flux is much less (the hollow object is not acting as a ramjet). Figure 10 presents the variation of cylinder drag coefficient (C_D) with both L/D and ID/OD ratios for ram-facing scenarios. There is a subtle difference in the slope of the contour lines between the three plots in Fig. 10 in the region near L/D = 0.5 and ID/OD = 0.5, indicating that the "hollowness" of an object is different depending on the rarefaction of the flow around the body.

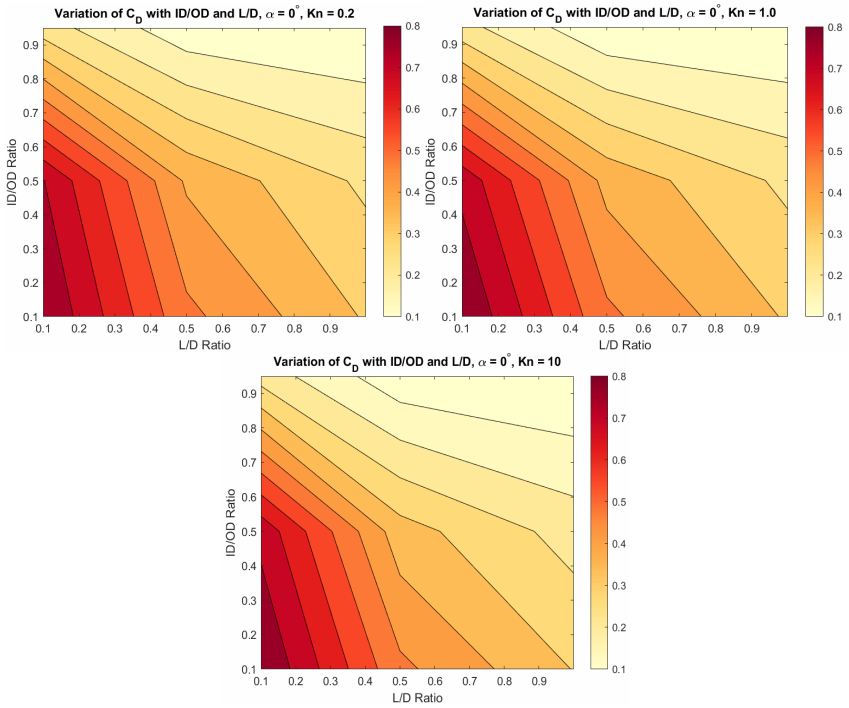

Fig. 10. Comparison of cylinder C_D variation with geometric ratios and Kn.

Finally, Fig. 11 illustrates the changes in the flowfield around and through a ram-facing, right-circular cylinder as the ID/OD ratio varies from 0.95 to 0.1, at Kn = 0.2. Between ID/OD values of 0.95 and 0.5, the peak centerline speed at the aft edge of the cylinder drops from 90% of the freestream speed to about 50%, causing a significant increase in drag. The peak centerline speed at the aft edge further drops to less than 10% of the freestream as the ID/OD ratio decreases to 0.1, to the point where the object can be treated as a solid.

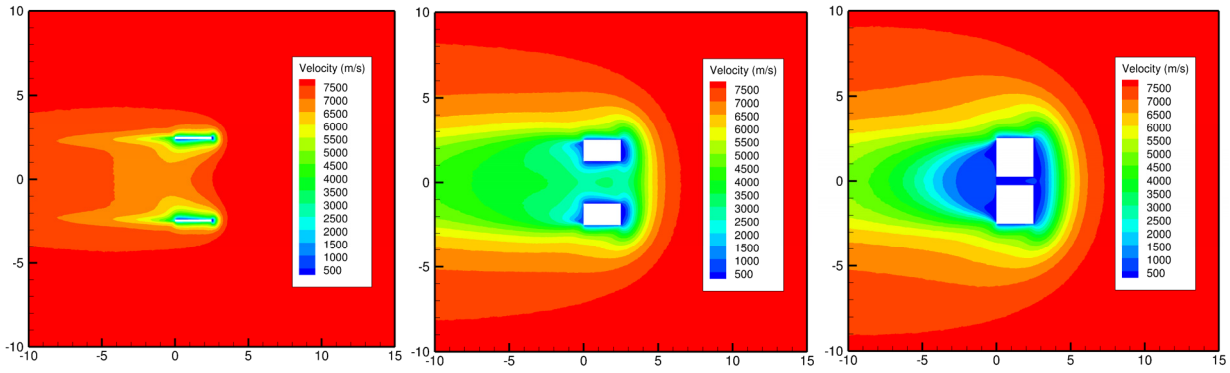

Fig. 11. ID/OD ratio-induced changes in DSMC-computed flowfield about a right-circular cylinder, Kn = 0.2.

4 CONCLUSIONS

DSMC simulations of simple hollow body shapes (cylinders and square rectangular prisms) were performed with the NASA DAC software at various angles of attack, wall thicknesses, and Kn within the transitional regime. The results were processed to determine drag and heating coefficients for each simulation. An attempt also was made to quantify the effect of the flow through the hollow body to establish a “hollowness” criterion. A sample of the preliminary results has been presented along with tabulated values that can be used as a rudimentary model in existing reentry-survivability analysis software. Future work will include additional transitional regime Kn, geometric ratios, and object orientations to more fully resolve the hollow body database and improve model accuracy.

5 References

1. Rochelle, W.C., *et al*. "Spacecraft Orbital Debris Reentry: Aerothermal Analysis,." Proceedings of the Eighth Annual Thermal and Fluids Analysis Workshop: Spacecraft Analysis and Design, Houston, 1-14 Oct., 1997.

2. Lips, T. and Fritsche, B. "A comparison of commonly used re-entry analysis tools," Acta Astronautica, pp. 312-323, 2005.

3. Boyles, K.A., *et al*. "The Use of Virtual Sub-Cells in DSMC Analysis of Orbiter Aerodynamics at High Altitudes Upon Re-entry," 41st Aerospace Sciences Meeting and Exhibit, Reno, Nevada, 2003.

4. Potter, J. L. and Peterson, S.W. "Local and Overall Aerodynamic Coefficients for Bodies in Hypersonic, Rarefied Flow," 29th Aerospace Sciences Meeting, Reno, NV, AIAA, 1991.

5. Turansky, C.P. "High-Fidelity Dynamic Modeling of Spacecraft in the Continuum–Rarefied Transition Regime," Boulder, CO,University of Colorado at Boulder, 2012.

6. Wilmoth, R. G., Blanchard, R.C., and Moss, J.N. "Rarefied Transitional Bridging of Blunt Body Aerodynamics," 21st International Symposium on Rarefied Gas Dynamics, Marseille, France, 1998.

7. Mehta, P.M., *et al*. "Sensitivity Analysis towards Probabilistic Re-Entry Modeling of Spacecraft and Space Debris," AIAA Modeling and Simulation Technologies Conference, Dallas, TX, AIAA, 2015.

8. Scanlon, T., *et al*. "Simulations of rarefied and continuum hypersonic flow over re-entry objects," 8th European Symposium on Aerothermodynamics for Space Vehicles, Lisbon, Portugal, ESA Conference Bureau, 2015.

9. LeBeau, G. J. and Lumpkin III, F.E. "Application Highlights of the DSMC Analysis Code (DAC) Software for Simluating Rarefied Flows," *Computer Models in Applied Mechanics and Engineering* 191.6-7: pp. 595-609, 2001.

10. Bird, G. A. *Molecular Gas Dynamics*. Oxford: Clarendon Press, 1976.

Appendix A. Table of Drag coefficients, Heating coefficients, and Hollowness Criteria

Parameters					Cylinder				Boxes			
Case #	Kn	L/D	ID/OD	α (°)	C_D	C_h	HC 1	HC 2	C_D	C_h	HC 1	HC 2
1	0.2	1	0.95	0	0.0932	0.0451	1.1208	1.0013	0.0953	0.0459	1.0977	0.9907
2	0.2	1	0.95	45	0.3337	0.1245	0.7292	0.6514	0.3191	0.1104	0.9579	0.8645
3	0.2	1	0.95	90	0.2890	0.0950	0.2062	0.1842	0.2762	0.0713	0.2482	0.2240
4	0.2	1	0.5	0	0.2730	0.0969	2.0402	0.5049	0.2748	0.0967	2.0559	0.5140
5	0.2	1	0.5	45	0.3482	0.1347	0.9731	0.2408	0.3317	0.1208	0.9704	0.2426
6	0.2	1	0.5	90	0.3101	0.1028	0.1446	0.0358	0.2958	0.0773	0.1832	0.0458
7	0.2	1	0.1	0	0.3451	0.0914	2.0514	0.0203	0.3478	0.0909	2.2414	0.0224
8	0.2	1	0.1	45	0.4066	0.1489	0.7060	0.0070	0.3858	0.1322	0.7863	0.0079
9	0.2	1	0.1	90	0.3651	0.1212	0.0176	0.0002	0.3480	0.0912	0.0382	0.0004
10	0.2	0.5	0.95	0	0.1126	0.0530	1.0990	0.9818	0.1166	0.0549	1.0812	0.9758
11	0.2	0.5	0.95	45	0.4054	0.1542	0.2627	0.2347	0.3729	0.1366	0.9170	0.8276
12	0.2	0.5	0.95	90	0.3010	0.1061	0.1679	0.1500	0.2875	0.0856	0.2238	0.2020
13	0.2	0.5	0.5	0	0.4061	0.1364	2.0476	0.5067	0.4075	0.1351	2.0598	0.5150
14	0.2	0.5	0.5	45	0.4284	0.1657	0.9181	0.2272	0.4110	0.1535	1.0358	0.2589
15	0.2	0.5	0.5	90	0.2786	0.0999	0.1221	0.0302	0.2656	0.0814	0.1531	0.0383
16	0.2	0.5	0.1	0	0.4975	0.1262	2.6658	0.0264	0.4996	0.1244	2.7733	0.0277
17	0.2	0.5	0.1	45	0.4639	0.1680	1.0416	0.0103	0.4448	0.1545	1.0922	0.0109
18	0.2	0.5	0.1	90	0.3006	0.1082	0.0159	0.0002	0.2861	0.0881	0.0361	0.0004
19	0.2	0.1	0.95	0	0.2526	0.1140	1.0822	0.9669	0.2570	0.1161	1.0763	0.9714
20	0.2	0.1	0.95	45	0.4764	0.2113	1.0704	0.9563	0.4340	0.1902	1.0435	0.9418
21	0.2	0.1	0.95	90	0.3094	0.1292	0.1499	0.1339	0.2812	0.1127	0.1967	0.1775
22	0.2	0.1	0.5	0	0.7428	0.2239	2.0806	0.5149	0.7437	0.2205	2.0925	0.5231
23	0.2	0.1	0.5	45	0.5707	0.2155	1.2149	0.3007	0.5564	0.2070	1.3139	0.3285
24	0.2	0.1	0.5	90	0.1675	0.0720	0.1006	0.0249	0.1572	0.0655	0.1382	0.0345
25	0.2	0.1	0.1	0	0.8041	0.1932	2.9345	0.0290	0.8033	0.1877	3.0152	0.0302
26	0.2	0.1	0.1	45	0.5744	0.1944	1.2124	0.0120	0.5626	0.1858	1.2727	0.0127
27	0.2	0.1	0.1	90	0.1504	0.0653	0.0176	0.0002	0.1423	0.0601	0.0214	0.0002
28	1	1	0.95	0	0.0858	0.0424	1.0923	0.9758	0.0855	0.0421	1.0755	0.9707
29	1	1	0.95	45	0.3609	0.1612	0.5745	0.5133	0.3315	0.1439	0.7249	0.6542
30	1	1	0.95	90	0.3133	0.1328	0.0215	0.0192	0.2814	0.1101	0.0388	0.0350
31	1	1	0.5	0	0.2720	0.1178	1.4225	0.3520	0.2749	0.1185	1.4329	0.3582
32	1	1	0.5	45	0.3889	0.1730	0.6697	0.1657	0.3599	0.1563	0.6873	0.1718
33	1	1	0.5	90	0.3349	0.1423	0.0065	0.0016	0.3012	0.1183	0.0213	0.0053

Parameters					Cylinder				Boxes			
34	1	1	0.1	0	0.3474	0.1356	0.6546	0.0065	0.3537	0.1369	0.7796	0.0078
35	1	1	0.1	45	0.4577	0.1999	0.1754	0.0017	0.4240	0.1802	0.2171	0.0022
36	1	1	0.1	90	0.3939	0.1673	0.0037	0.0000	0.3543	0.1392	0.0048	0.0000
37	1	0.5	0.95	0	0.0972	0.0469	1.0723	0.9580	0.0986	0.0475	1.0613	0.9578
38	1	0.5	0.95	45	0.4287	0.1926	0.4903	0.4380	0.3776	0.1670	0.7659	0.6912
39	1	0.5	0.95	90	0.3169	0.1379	0.0109	0.0097	0.2810	0.1160	0.0254	0.0229
40	1	0.5	0.5	0	0.4002	0.1700	1.4622	0.3618	0.4022	0.1697	1.4696	0.3674
41	1	0.5	0.5	45	0.4683	0.2090	0.6421	0.1589	0.4404	0.1937	0.7823	0.1956
42	1	0.5	0.5	90	0.2906	0.1268	0.0094	0.0023	0.2591	0.1076	0.0134	0.0033
43	1	0.5	0.1	0	0.5051	0.1951	1.2219	0.0121	0.5100	0.1949	1.3428	0.0134
44	1	0.5	0.1	45	0.5104	0.2220	0.4109	0.0041	0.4822	0.2060	0.4666	0.0047
45	1	0.5	0.1	90	0.3130	0.1368	0.0010	0.0000	0.2792	0.1161	0.0024	0.0000
46	1	0.1	0.95	0	0.2412	0.1134	1.0530	0.9408	0.2425	0.1140	1.0487	0.9465
47	1	0.1	0.95	45	0.4995	0.2356	1.0157	0.9074	0.4408	0.2065	0.9605	0.8669
48	1	0.1	0.95	90	0.3145	0.1449	0.2239	0.2000	0.2729	0.1238	0.2445	0.2206
49	1	0.1	0.5	0	0.7385	0.3046	1.5088	0.3734	0.7408	0.3032	1.5154	0.3788
50	1	0.1	0.5	45	0.6024	0.2670	1.0103	0.2500	0.5841	0.2570	1.0359	0.2590
51	1	0.1	0.5	90	0.1564	0.0726	0.1356	0.0336	0.1393	0.0638	0.1600	0.0400
52	1	0.1	0.1	0	0.8270	0.3163	1.7276	0.0171	0.8283	0.3126	1.8383	0.0184
53	1	0.1	0.1	45	0.6151	0.2619	0.7556	0.0075	0.6034	0.2541	0.0002	0.0000
54	1	0.1	0.1	90	0.1376	0.0641	0.0333	0.0003	0.1235	0.0568	0.0001	0.0000
55	10	1	0.95	0	0.0590	0.0288	0.9675	0.8643	0.0587	0.0287	0.9582	0.8648
56	10	1	0.95	45	0.3911	0.1880	0.7461	0.6665	0.3495	0.1668	0.7264	0.6556
57	10	1	0.95	90	0.3275	0.1546	0.7069	0.6315	0.2710	0.1258	0.6690	0.6038
58	10	1	0.5	0	0.2398	0.1124	0.9041	0.2237	0.2403	0.1125	0.9075	0.2269
59	10	1	0.5	45	0.4232	0.2022	0.6971	0.1725	0.3807	0.1806	0.6924	0.1731
60	10	1	0.5	90	0.3490	0.1648	0.6610	0.1636	0.2888	0.1341	0.6383	0.1596
61	10	1	0.1	0	0.3363	0.1558	0.4619	0.0046	0.3374	0.1558	0.4792	0.0048
62	10	1	0.1	45	0.4988	0.2378	0.6711	0.0066	0.4491	0.2124	0.6827	0.0068
63	10	1	0.1	90	0.4103	0.1938	0.6535	0.0065	0.3394	0.1577	0.6326	0.0063
64	10	0.5	0.95	0	0.0806	0.0390	0.9761	0.8720	0.0807	0.0390	0.9749	0.8799
65	10	0.5	0.95	45	0.4510	0.2174	0.9544	0.8527	0.3837	0.1839	0.9591	0.8656
66	10	0.5	0.95	90	0.3286	0.1559	1.0215	0.9126	0.2727	0.1276	1.0245	0.9246
67	10	0.5	0.5	0	0.3689	0.1724	0.7649	0.1893	0.3695	0.1724	0.7535	0.1884
68	10	0.5	0.5	45	0.5068	0.2424	0.8861	0.2193	0.4694	0.2234	0.8871	0.2218
69	10	0.5	0.5	90	0.2989	0.1420	1.0230	0.2532	0.2482	0.1163	1.0276	0.2569
70	10	0.5	0.1	0	0.4960	0.2292	0.5916	0.0059	0.4965	0.2288	0.5560	0.0056
71	10	0.5	0.1	45	0.5502	0.2619	0.8553	0.0085	0.5116	0.2422	0.8490	0.0085
72	10	0.5	0.1	90	0.3217	0.1528	1.0247	0.0101	0.2671	0.1252	1.0273	0.0103
73	10	0.1	0.95	0	0.2376	0.1134	0.9883	0.8829	0.2371	0.1132	0.9885	0.8921
74	10	0.1	0.95	45	0.5128	0.2481	0.9928	0.8870	0.4470	0.2153	0.9926	0.8958
75	10	0.1	0.95	90	0.3270	0.1566	1.0028	0.8959	0.2776	0.1318	1.0054	0.9074
76	10	0.1	0.5	0	0.7380	0.3439	0.8962	0.2218	0.7378	0.3431	0.8833	0.2208
77	10	0.1	0.5	45	0.6348	0.3027	0.9555	0.2365	0.6116	0.2908	0.9513	0.2378
78	10	0.1	0.5	90	0.1527	0.0734	1.0033	0.2483	0.1303	0.0622	1.0064	0.2516
79	10	0.1	0.1	0	0.8294	0.3826	0.8332	0.0082	0.8286	0.3811	0.8077	0.0081
80	10	0.1	0.1	45	0.6555	0.3106	0.9329	0.0092	0.6409	0.3028	0.9249	0.0092
81	10	0.1	0.1	90	0.1325	0.0638	1.0081	0.0100	0.1131	0.0541	1.0059	0.0101